RESEARCH PAPER

Prussian blue-doped nanosized polyaniline for electrochemical detection of benzenediol isomers

Bhargav R. Patel[1] · Meissam Noroozifar[1] · Kagan Kerman[1]

Abstract

Simultaneous speciation of benzenediol isomers (BDIs), 1,2-benzenediol (catechol, CC), 1,3-benzenediol (resorcinol, RS), and 1,4-benzenediol (hydroquinone, HQ), was investigated by differential pulse voltammetry (DPV) using a graphite paste electrode (GPE) modified with Prussian blue-polyaniline nanocomposite. The modified GPE showed good stability, sensitivity, and selectivity properties for all the three BDIs. Prussian blue-doped nanosized polyaniline (PBNS-PANI) was synthesized first by using mechanochemical reactions between aniline and ferric chloride hexahydrate as the oxidants and then followed by the addition of potassium hexacyanoferrate(II) in a solid-state and template-free technique. The material was characterized by scanning electron microscopy, transmission electron microscopy, Fourier transform infrared spectroscopy (FT-IR), and X-ray photoelectron spectroscopy (XPS). The DPV measurements are performed in phosphate electrolyte solution with pH 4.0 at a potential range of − 0.1 to 1.0 V. The proposed modified electrode displayed a strong, stable, and continuous three well-separated oxidation peaks towards electrooxidation at potentials 0.20, 0.31, and 0.76 V for HQ, CC, and RS, respectively. The calibration curves were linear from 1 to 350.5 μM for both HQ and CC, while for RS, it was from 2 to 350.5 μM. The limit of detection was determined to be 0.18, 0.01, and 0.02 μM for HQ, CC, and RS, respectively. The analytical performance of the PBNS-PANI/GPE has been evaluated for simultaneous determination of HQ, CC, and RS in creek water, commercial hair dye, and skin whitening cream samples with satisfactory recoveries between 90 and 106%. Overall, we demonstrated that the presence of NS-PANI and PB resulted in a large redox-active surface area that enabled a promising analytical platform for simultaneous detection of BDIs.

Keywords Catechol · Hydroquinone · Resorcinol · Graphite paste electrode · Differential pulse voltammetry

Introduction

Rapid and sensitive detection of organic pollutants having structural isomers is of a significant concern in environmental monitoring studies [1–3]. The benzenediol isomers (BDI), catechol (1,2-benzenediol, CC), resorcinol (1,3-benzenediol, RS), and hydroquinone (1,4-benzenediol, HQ) (see Scheme 1), are widely present in the environment because of the commercial mass production and vast potential applications. They are used as industrial solvents or as raw materials in several industries [3, 4] and are also found in industrial effluents as they are extensively used in production of food additives, hair dyes, rubber, plastics, synthetic fibers, paper, cosmetics, and pharmaceuticals [4–8]. These isomers are also found from the wastewater effluents of several industrial processes such as synthetic coal fuel conversion, coal-tar production, photo-processing, steel, paper, and pulp mills in concentrations ranging from 1 to 1000 mg/l [4]. Upon its toxicological assessment due to health concerns, Health Canada has classified HQ and CC to be "toxic" under Canadian Environmental Protection Act, 1999 [9, 10]; in addition, it has also listed all the three BDI under the List of Prohibited and Restricted Cosmetic Ingredients (Cosmetic Ingredient Hotlist) [11]. The removal of BDI is necessary due to their low degradability, high toxicity, and high oxygen demand in the ecological environment. Moreover, due to these reasons, national environmental agencies from the USA, European Union, and Canada have classified them as primary

✉ Kagan Kerman
kagan.kerman@utoronto.ca

[1] Department of Physical and Environmental Sciences, University of Toronto Scarborough, 1265 Military Trail, Toronto, ON M1C 1A4, Canada
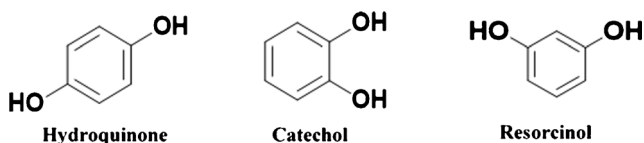
Scheme 1 The chemical structures of BDI

wastewater pollutants [4, 12, 13]. Previous reports have shown the ability of CC to foster DNA damage and stimulate tumors and its toxicity for microorganisms, water flea, human cell lines, zebra fish, and trout [4, 14, 15]. HQ and RS are also widely used in cosmetic and pharmaceutical creams and lotions for topical applications on skin. Although the data for carcinogenicity of HQ and RS on humans is insufficient, several studies have shown that HQ can augment the spread of lung cancer and is toxic primarily in kidney and stomach and RS triggers serious neurological complications such as angioneurotic edema along with eczema and urticaria [4, 16].

Furthermore, the structural similarity and physiochemical characteristics of BDI induce it to co-exist in environmental samples and cause interference during its detection [3, 5]. Until now, several analytical methods have been established for detection of BDI such as colorimetric [5], liquid chromatography-tandem mass spectrometry [17], gas chromatography-mass spectrometry [18], electrochemistry [19], spectroelectrochemistry [20], chemiluminescence [21], fluorescence [22], capillary electrophoresis [23], spectrophotometry [3], and phosphorescence [1]. Amongst these, the chromatographic and spectrometric methods are quantitative and have good sensitivity, but they are time-consuming due to the laborious sample pre-treatment and preparation steps, require highly skilled personnel, have high instrumentation cost, and cannot be used on-site for analysis [5, 24]. In contrast, the electrochemical methods are most widely used because of their sensitivity, low cost, miniaturization capabilities, and rapid detection [5]. Earlier Lisdat et al. [25] have used enzymatic amplification sensors using the principle of substrate recycling for detection of catechol derivatives, and in another past study by Mizutani et al. [26], the amplification biosensor performance for HQ, CC, and other dihydroxyphenols was improved by utilizing the bioelectrocatalytic recycling approach. Furthermore, Niwa et al. [27, 28] had also used electrodes modified by molecular imprinting technique and interdigitated array microelectrodes for electrochemical detection of the catechol and catecholamines. Recently, few studies have used various modifiers on different types of electrode materials for electrochemical determination of BDI. For example, electrodes modified with hybrid material made up of reduced graphene oxide-multiwall carbon nanotubes was used by Hu et al. [29] for simultaneous determination of BDI. Tian et al. [30] had used one-dimensional poly (3,4-ethylenedioxythiophene)-graphene composites-based electrochemical sensors for determination of BDI. Moreover, Tohidinia et al. [19] used graphite paste electrodes modified

with poly(quercetin)-bismuth nanowires for simultaneous determination of the HQ, CC, and RS. Also, glassy carbon electrode modified with nanoraspberry-like copper/reduced graphene oxide nanocomposites was used by Sabbaghi and Noroozifar [31] for detection of HQ, CC, and RS, recently.

Polyaniline (PANI) a conducting electroactive polymer has recently shown promising potential in fabrication of anti-corrosion coatings, batteries, and electrochemical biosensors due to its distinctive electronic and optical characteristics, redox properties, cost-effectiveness, ease of synthesis, high conductivity, environmental stability, and facile doping mechanisms [32]. Previous studies have also demonstrated that these properties of PANI can be enhanced by incorporation of metal nanoparticles, hexacyanoferrates, and other functional materials [33]. Polyaniline-based sensors have earlier been reported by Bartlett and Ling-Chung [34] as intelligent gas sensors for different vapors. Kilmartin et al. [35] have reported the use of polyaniline-based sensors for electrochemical detection of ascorbic acid in beverages. Prussian blue (PB) is another redox material with good stability, conductivity, and electrocatalytic properties [36]. The first reported use of PB-modified electrodes was by Karyakin et al. [37] who used it as amperometric sensors for detection of glucose. Several studies have reported the use of metal oxide-based and nanoparticle-based electrochemical sensors for BDI detection, but there have been only a few reports on PB-based BDI detection. Recently, Buleandra et al. [38] had used an electrochemically activated and PB-modified screen-printed electrode for simultaneous detection of HQ and CC; however, RS was not detected simultaneously in this study. In environmental water samples, the three BDI might co-exist as pollutants. In environmental water samples, the three BDI might co-exist as pollutants; therefore, detecting all the three BDIs simultaneously using a modified electrode can have a wide analytical scope. It has been hypothesized previously [39, 40] that PANI-PB hybrid would produce synergistic effects from the two electroactive materials that is not possible from each of the single components. Nonetheless, it is still motivating to study novel electrode modifications for simultaneous detection of the BDIs.

Ideally to start the remedial actions swiftly and prevent any environmental incidents due to the contaminants, it becomes imperative to develop simple, reliable, cost-effective, rapid, selective and sensitive method for early detection and discrimination of pollutants such as BDIs. The goal of this work was to develop a nanocomposite-based electrochemical sensor for simultaneous detection of HQ, CC, and RS using PB-PANI hybrid-modified GPE. This type of electrode will possess characteristics such as low cost, good stability, rapid response, good selectivity, and low detection limits. To the best of our knowledge, no study has been reported on the speciation and simultaneous analysis of HQ, CC, and RS using a modified GPE with PBNS-PANI nanocomposite. In the present study, for the first time, nanosized polyaniline (NS-PANI) was

synthesized using one step in situ mechanochemical reaction method from aniline and iron(III) chloride salt. This polymer was doped with Prussian blue (PB) and then used for preparation of the modified graphite paste electrode (GPE). The proposed modified electrode, PBNS-PANI/GPE, was used as a new and sensitive electrode for speciation of HQ, CC, and RS in creek water (Highland creek, Scarborough, ON), commercial hair dye and skin whitening cream samples. The results showed that in situ mechanochemical synthesis of the modifier without any pre-treatment, pre-concentration, or separation methods helped in achieving good stability, low detection limits, and excellent selectivity.

Experimental

Reagents and solutions

Hydroquinone (HQ), catechol (CC), resorcinol (RS), aniline (AN), and iron(III) chloride were purchased from Sigma-Aldrich (Oakville, ON) and used without further purification. A series of electrolyte solutions including H_3PO_4 (0.2 M) were prepared and pH adjusted using NaOH (0.1 M) in the range from 2.0 to 8.0. All the reagent solutions were freshly made for each measurement in 18.2 MΩ purified water (Millipore, Darmstadt, Germany). All measurements were performed in compliance with the relevant laws and institutional guidelines.

Instrumentation and characterization

Cyclic voltammetry (CV), differential pulse voltammetry (DPV), and electrochemical impedance spectroscopy (EIS) were performed using an µAutolab PGSTAT 128 N (Eco Chemie, Netherlands) potentiostat/galvanostat powered by NOVA 2.0 software. In addition, a conventional three-electrode cell was used while all the electrochemical measurements were performed, where the (PBNS-PANI/GPE) modified electrode was the working electrode, a platinum electrode was the counter electrode, and an Ag/AgCl electrode in saturated KCl was the reference electrode. Moreover, 10 mM $[Fe(CN)_6]^{3-/4-}$ prepared in 0.1 M KCl was used while performing the EIS measurements over a frequency range of 0.1 Hz to 10 kHz with 0.02 V amplitude (rms). DPV measurements were performed in a wide potential window from − 0.1 to 1.0 V at a step potential of 5 mV and a modulation amplitude of 0.025 V with a modulation time of 0.05 s as well as an interval time of 0.5 s. A Metrohm Titrando pH meter (model 888) was used for pH measurements. SEM analyses of the samples were performed using a Quanta FEG 250 ESEM™ scanning electron microscope from FEI Company (Minato, Japan). UV-activated carbon coated copper mesh grid (Electron Microscopy Sciences, Hatfield, PA) was spot coated

with PBNS-PANI and blot dried for 15 min. The Hitachi H-7500 transmission electron microscope (Hitachi, Japan) was then used to image the prepared samples and determine its topography. FT-IR spectral analysis was performed using Bruker alpha-P FT-IR spectrometer (Billerica, MA) equipped with a highly sensitive deuterated lanthanum α alanine doped triglycine sulphate (DLaTGS) detector. A FT-IR spectrum was obtained by placing powdered PB, NS-PANI, and PBNS-PANI on the crystal. FT-IR spectra were obtained at a resolution of 2 cm^{-1} at a scan rate of 16, between 4000 and 400 cm^{-1}. FT-IR spectra were baseline corrected and smoothened once with an average of 17 data points. All the data analysis was performed with Opus 6.5® software. ThermoFisher Scientific K-Alpha X-ray photoelectron spectrometer (ThermoFisher Scientific—E. Grinstead, UK) was used to perform all the XPS measurements. Low resolution survey spectra (nominal 900 µm spot, 100 eV pass energy), followed by high-resolution spectra (nominal 900 µm spot, 100 eV pass energy) for all of the elemental regions observed on the NS-PANI and PBNS-PANI samples were collected. The system's combined e^-/Ar^+ floodgun was used to apply the charge compensation. All data processing was performed using the software supplied with the system (Avantage™ 5.926).

Preparation of NS-PANI and PB-doped NS-PANI

The preparation of NS-PANI was carried out by hand-grounding and mixing 10 mM aniline and 20 mM FeCl$_3$·6H$_2$O for 2 min. The mixture developed a black color, which was from the FeCl$_3$·6H$_2$O. Upon further grinding for about 8 min, the mixture was changed from powder to slurry. Once it turned slurry, the mixture was further grinded which resulted in the slurry to turn green in color, which indicated the formation of NS-PANI in its doped emeraldine salt (ES) oxidation state and the reduction of Fe^{3+}. Next, this mixture was grinded for additional 40 min, and then the product was collected and purified by washing with water and filtering using a Buchner funnel connected to a water aspirator. Finally, the products were dried at room temperature and mixed then with $K_4Fe(CN)_6$ solution. The final product, PBNS-PANI composite, was again washed with water and dried at 70 °C in oven for 1 h. Based on these results, the mechanism of the synthesis is illustrated in Scheme 2. In this reaction, FeCl$_3$.6H$_2$O was used as oxidant for the polymerization of aniline, during the polymerization, Fe^{3+} was reduced to Fe^{2+} and resulted in the subsequent formation of NS-PANI. After the polymerization, Fe^{3+} ions were still in the medium of reaction as observed in the XPS spectra (Fig. 2d) of NS-PANI as the amount of oxidant was five times the amount of monomer. In the final step, the PB were prepared with adding $K_4Fe(CN)_6$ solution in the ambient air and the doped PB in NS-PANI (PBNS-PANI) were formed.
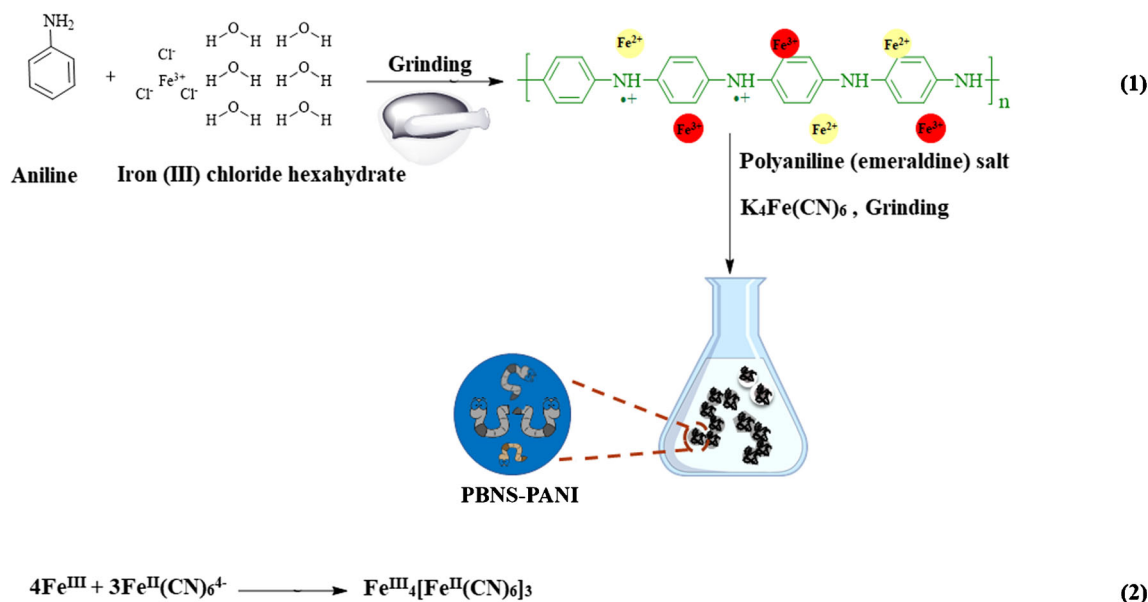
Scheme 2 Schematic illustration for the synthesis of Prussian blue-doped nanosized polyaniline (PBNS-PANI) using aniline and ferric chloride hexahydrate as the oxidants followed by the addition of potassium hexacyanoferrate(II) in a solid-state and template-free technique

Preparation of NS-PANI/GPE and PBNS-PANI/GPE modified electrodes

NS-PANI or PBNS-PANI (6 mg) and graphite (194 mg) were thoroughly mixed stoichiometrically and transferred into a mortar, where 5 mg of paraffin oil was added to the mixture. Next, this mixture was grounded using a pestle for 10 min. Following this, glass tubes with a 2-mm diameter were filled either using the prepared NS-PANI or PBNS-PANI modified graphite paste and then an electrical contact was created by inserting a copper wire into the glass tube. Similarly, for un-modified GPE electrode, graphite (200 mg) was used to create the graphite paste as mentioned earlier. A new surface of the GPE was re-generated by pushing the graphite paste out of the glass tube and polishing the electrode with printing paper. All the prepared electrodes were next placed in 0.2 M phosphate electrolyte solution at pH 4.0, and the electrode potential was cycled between -0.2 and 1.0 V (vs. Ag/AgCl) at a scan rate of 50 mV s^{-1} for 10 cycles in a cyclic voltammetry regime until a stable voltammogram was attained. The modified electrodes were stored in deionized distilled water, when not in use.

Real sample analysis

The potential applicability of the proposed sensor was examined by detecting benzenediol isomers in real-life samples. Specifically, the performance of the proposed sensor was tested in various matrices such as creek water (Highland creek, Scarborough, ON), 1% (w/v) commercial hair dye and 1% (w/v) skin whitening cream solutions. Various matrices were spiked with varying concentrations of CC, HQ, or RC and

then, the BDI were detected using the aforementioned analyses in triplicates ($n = 3$).

Results and discussions

Morphological and spectroscopic characterization

A conducting polymer such as PANI is reported to have unique electrical and optical properties due to their polymer backbone possessing a π electron delocalization [41]. PANI can exist either in a fully reduced state as, non-conductive, leucoemeraldine (LE) or in half oxidized state as, non-conductive, emeraldine base. It can also exist as either a fully oxidized, non-conductive, pernigraniline (PE) state or as a conductive emerdaline salt (ES) state [42–44]. Doping and deprotonation are known to control the electric and optical properties of PANI [41]. It has been reported earlier by the MacDiarmid group that the resulting PANI becomes non-electroactive if the pH of the polymerization reaction is more than 4 because the ES salt is not formed [45]. Past reports have shown that the optical properties of the PANI are related to their redox states where the most reduced LE form is in yellow color, the half oxidized emeraldine base is in blue color, the fully oxidized pernigraniline appears purple in color, and the emeraldine salt appears as green color [42, 44, 45]. The corresponding FT-IR spectra for the PB, NS-PANI, and PBNS-PANI are shown in Fig. 1. In both FT-IR spectra for the NS-PANI and PBNS-PANI, the absorption at 3200–3500 cm^{-1} is assigned to the of the N-H stretching bond of the phenyl ring. In addition, three important absorption peaks for N-H band of primary amines, C-N stretching, and N-H wag of primary

amines can be assigned from the absorption bands detected at 1619, 1277, and 764 cm^{-1}, respectively. FT-IR spectrum of PBNS-PANI (Fig. 1a) showed a broad band at wavenumbers higher than 2000 cm^{-1}; this was characteristic for complete doping and conducting form. Moreover, the peak at 1574 cm^{-1} was ascribed to C=N stretching modes for the quinoid, and the peak at 1486 cm^{-1} was typical of C=C stretching mode for the benzenoid rings. The peak at 1298 cm^{-1} was due to stretching vibration of aromatic C–N, which also indicated a π-electron delocalization in system. Finally, the two bands typical of the conducting emeraldine salt were also observed at 1248 and 1134 cm^{-1} [46–48]. As shown in Fig. 1b, SEM image demonstrated that the PBNS-PANI had an average size of 50 ± 5.0 nm, which consisted of several small nanoparticles that would increase the redox-active surface area. As shown in TEM images in Fig. 1c and d, the morphology of the obtained products revealed approximately similar in size and had spherical/oval shapes.

X-ray photoelectron spectroscopy (XPS) measurements were carried out to confirm the valence states of the elements present in the binary PBNS-PANI nanocomposite. Fig. S1 (see Electronic Supplementary Material (ESM)) shows the XPS survey spectra of PBNS-PANI and NS-PANI alone, which revealed the presence of Fe, C, Cl, O, and N elements in the nanocomposite. Higher resolution spectra (Fig. 2a–e) for the constituent elements helped in further understanding of the electronic states of the respective elements. The high-resolution XPS spectra of N 1s of nitrogen showed three characteristic strong peaks at 398.42 and weak peaks at 399.73, and 401.18 eV for the NS-PANI and a strong peak at 397.93 and weak peaks at 399.66, and 401.08 eV for PBNS-PANI. For both NS-PANI and PBNS-PANI, the aforementioned peaks were ascribed to the imine N, amine N, and positively charged N, respectively [49, 50]. The presence of a weak peak at ~401 eV, characteristic of positively charged N, in both NS-PANI and PBNS-PANI implied that the PANI was in its protonated state [49]. As reported earlier by Tang et al. [50] and Wei et al. [51], the characteristic peak of imine at ~398 eV belongs to the imine group from the emeraldine as shown in Fig. 2(e). Moreover, the emergence of the peak at 397.93 eV indicated the presence of the C≡N from PB and the peak at 399.66 eV indicated the presence of aniline N in the hybrid of PBNS-PANI, which is in good agreement as reported by Muthusamy and Charles [52]. Furthermore, the increase in the peak intensity of N at 396.69 eV in the PBNS-PANI nanocomposite compared to NS-PANI indicated that the degree of protonation was greater in the nanocomposite [49]. The higher resolution XPS spectra of Fe 2p in the PBNS-PANI nanocomposite showed two characteristic peaks at 712.87 and 725.77 eV for Fe 2p$_{3/2}$ and Fe 2p$_{1/2}$, respectively, which were attributed to the presence of the ferric ion [52]. The peak observed at 708.67 eV was attributed to the presence of [Fe(CN)$_6$]$^{3-/4-}$ from Fe 2p$_{3/2}$ [52, 53]. From the higher

resolution XPS spectra of C 1s from the PBNS-PANI nanocomposite, it was observed that there were three deconvoluted peaks at 284.83, 286.15, and 287.37 eV, which were characteristic of C–C, C–N, and C=O bonding, respectively, and were in good agreement with literature [52, 54]. Therefore, the presence of PB was established in the proposed PBNS-PANI nanocomposite. Finally, from the higher resolution XPS spectra of Cl, it was observed that the chloride peak at 197.30 eV observed in NS-PANI was absent in the spectra of PBNS-PANI nanocomposite, which indicated the removal of chloride ions from the nanocomposite to enable the formation of the cyanide bridge via the movement of chloride ions in the NS-PANI matrix [49]. Overall, the results from XPS measurements further indicated that the PB was present in the PBNS-PANI nanocomposite.

Electrochemical characterization of PB/GPE, NS-PANI/GPE, and PBNS-PANI/GPE electrodes

The cyclic voltammograms (CVs) of GPE and different modified (PB/GPE, NS-PANI/GPE, and PBNS-PANI/GPE) electrodes carried out in 10 mM [Fe(CN)$_6$]$^{3-/4-}$ in 0.1 M KCl supporting electrolyte are shown in Fig. 3A. Based on Fig. 3A, the ΔE_p for GPE, PB/GPE and NS-PANI/GPE, and PBNS-PANI/GPE are 0.30, 0.29, 0.27, and 0.26 V, respectively. The results showed a decrease in the ΔE_p in the following order: GPE > PB/GPE > NS-PANI/GPE > PBNS-PANI/GPE.

Moreover, EIS technique was used as a supportive proof to confirm the CV results and to study the electrode-electrolyte interfacial features by determining the impedance or charge transfer resistance (R_{ct}) values of electrodes in step-wise modification of GPE [55]. Furthermore, [Fe(CN)$_6$]$^{3-/4-}$ was used a redox probe and the Nyquist plots for modified electrodes with frequency ranging from 0.1 Hz to 10 kHz were obtained (Fig. 3B). The fitting and the simulation of the obtained EIS data was performed using NOVA™ software. The modified Randles circuit shown as an inset in Fig. 3B was chosen as the equivalent circuit and was used for the fitting and simulation studies. As shown in Fig. 3B, the Nyquist plots of GPE, PB/GPE, NS-PANI/GPE, and PBNS-PANI/GPE contained two parts. The semicircle at higher frequencies, in which the diameter displayed the R_{ct}, which signaled the charge transfer limitations, followed by a straight line, which was observed in the lower frequencies due to the mass transfer limitations [19, 55]. The R_{ct} values for PBNS-PANI/GPE, NS-PANI/GPE, PB/GPE, and GPE were 493.5, 994.5, 1530, and 1840 Ω, respectively. The large semicircle diameter obtained for GPE indicated a R_{ct} to the [Fe(CN)$_6$]$^{3-/4-}$ probe in the electrolyte solution. The R_{ct} was decreased when the PB and NS-PANI were used as modifier in GPE (PB-GPE and NS-PANI/GPE), these are attributed to the conductive nature of PB and NS-PANI. This result emphasizes the fact that PB and NS-PANI can assist in electron transfer mechanism. Interestingly, after

Fig. 1 **a** FT-IR spectra of NS-PANI, PB, and PBNS-PANI; **b** SEM of PBNS-PANI; **c**, **d** TEM of PBNS-PANI
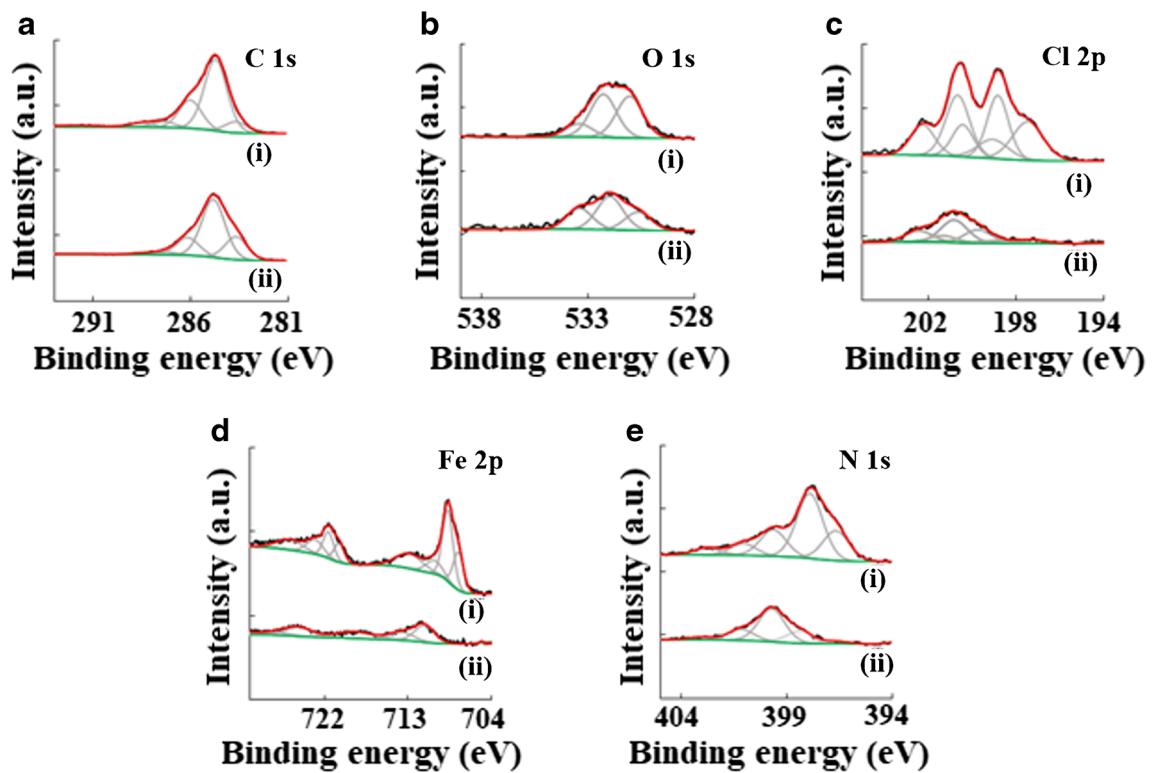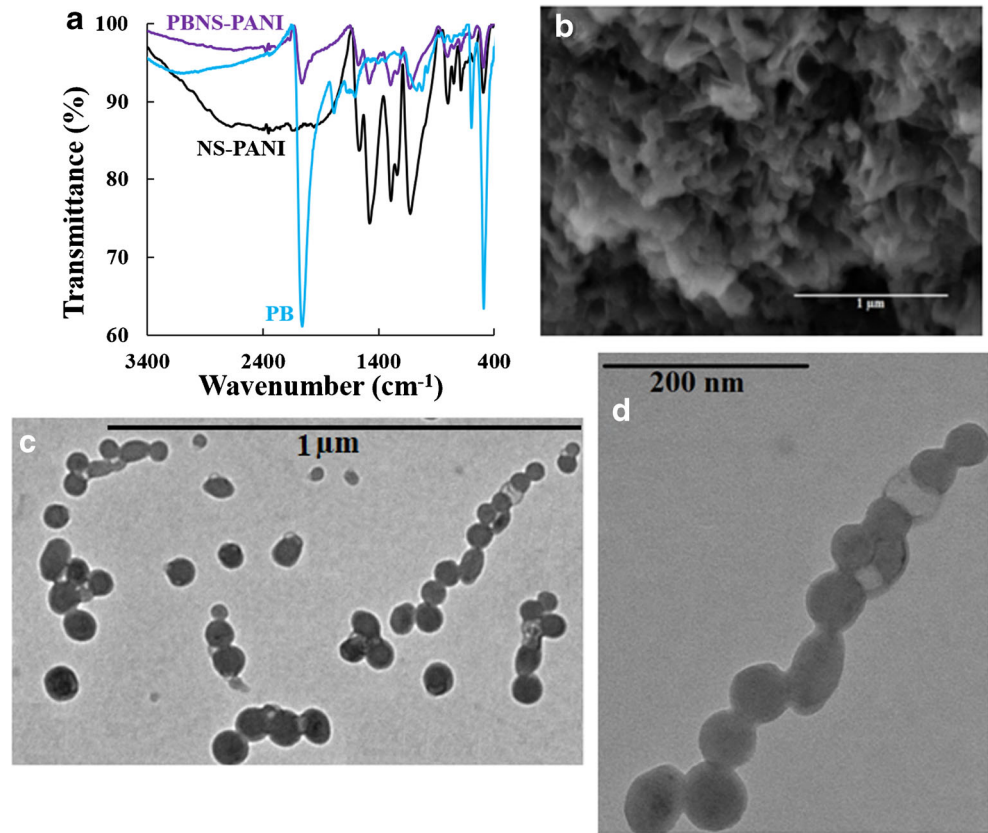
Fig. 2 Photoelectron analyses showing high-resolution spectra of NS-PANI (i) and PBNS-PANI (ii): **a** C 1s spectra, **b** O 1s spectra, **c** Cl 2p spectra, **d** Fe 2p spectra, and **e** N 1s

Fig. 3 (**A**) Cyclic voltammograms of PBNS-PANI/GPE, NS-PANI/GPE, PB/GPE, and GPE in 10 mM $[Fe(CN)_6]^{3-/4-}$ containing 0.1 M KCl at a scan rate of 100 mVs^{-1}. (**B**) Nyquist plots of (**a**) PBNS-PANI/GPE, (**b**) NS-PANI/GPE, (**c**) PB/GPE, and (**d**) GPE in 10 mM $[Fe(CN)_6]^{3-/4-}$ containing 0.1 M KCl; (**B** inset) modified Randles equivalent circuit. R_s: solution resistance, R_{ct}: charge transfer resistance, W: Warburg element, C_{dl}: double layer capacitance
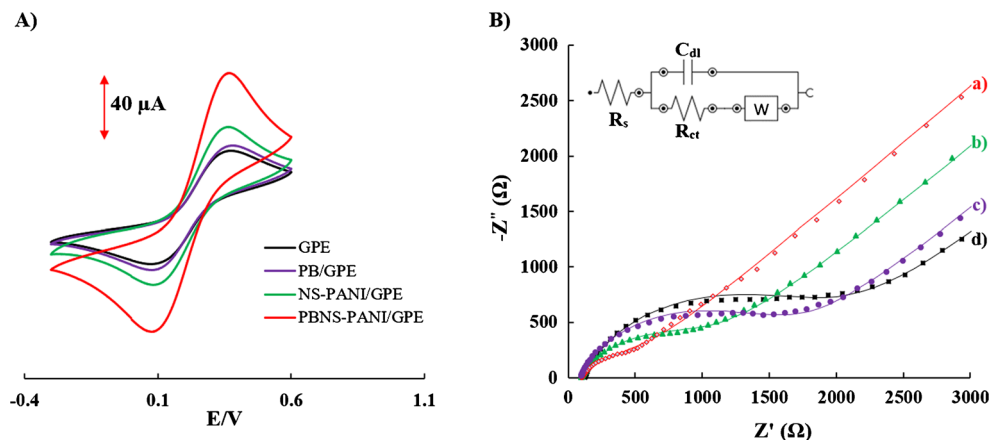
using both PB and NS-PANI as modifier in GPE (PBNS-PANI/GPE), the R_{ct} decreased in comparison to other mentioned electrodes. It can be ascribed to the surrounding of the PB particles by the formed NS-PANI polymer matrix which increased the electron transfer. Therefore, this proved that the PBNS-PANI can perform as an excellent electronic substrate and can ameliorate the surface area and electron transfer processes.

Moreover, the electrochemistry of PB-PANI nanocomposite was characterized by performing CVs of NS-PANI/GPE, PB/GPE, and PBNS-PANI/GPE in 0.1 M KCl solution at a scan rate of 100 mV s^{-1}. The peak at 0.72 V depicts the oxidation peak for PANI (emeraldine form) in NS-PANI/GPE. The peak at 0.22 V depicts the oxidation peak for PB in PBNS-PANI/GPE. For PBNS-PANI/GPE, a broad peak was observed at around 0.27 V, which can be assigned to PB present in the PBNS-PANI hybrid. The broad nature of the CV peak is in good agreement with the literature [49], and it appears broad as the PANI matrix lowers the diffusion of K$^+$ ions into PB, which otherwise is shown at 0.22 V for only PB as shown in Fig. S2 (see ESM). Therefore, a PB network is indicated to appear in the PANI matrix. Furthermore, in order to obtain the effective area (A) of the modified electrodes, electrochemical measurements of the PBNS-PANI/GPE, NS-PANI/GPE, PB/GPE, and GPE were performed using the CV method and the data was analyzed for the anodic peak current (I_{pa}) obtained from the respective CVs in the presence of 10 mM of $[Fe(CN)_6]^{3-/4-}$ in 0.1 M KCl of supporting electrolyte (Fig. S3, see ESM). All assays were completed using CV between potentials of -0.3 to 0.8 V as a probe at different scan rates. For a reversible process, the following Randles–Sevcik equation can be used [19, 56]:

$$i = (2.69 \times 10^5) n^{3/2} D^{1/2} C A v^{1/2} \qquad (1)$$

where I_{pa} refers to the anodic peak current, n is the electron transfer number, A is the surface area of the electrode, D is the diffusion coefficient, C is the concentration of $[Fe(CN)_6]^{3-/4-}$, and v is the scan rate. For $[Fe(CN)_6]^{3-/4-}$, $n = 1$, and $D = 7.6 \times$

10^{-6} cm s^{-1}, the effective surface areas of the electrodes can be calculated from the slope of the I_{pa}–$v^{1/2}$ relation. For GPE, PB/GPE, NS-PANI/GPE, and PBNS-PANI/GPE, the electrode surface was found to be 0.010, 0.038, 0.069, and 0.084 cm^2, respectively. This indicated that the effective surface area of PBNS-PANI/GPE was about 87, 54, and 18% more than GPE, PB/GPE, and NS-PANI/GPE. Therefore, the voltammetric and impedance results emphasized that the hybrid of PB together with NS-PANI, greatly improved the effective surface area of the electrode and improved the conductivity of the sensor.

Electrochemical behavior of the benzenediol isomers

The electrochemical performance of the mixture of analytes containing HQ, CC, and RS in 0.2 M phosphate electrolyte solution at pH 4.0 was investigated at the surfaces of GPE, PB/GPE, NS-PANI/GPE, and PBNS-PANI/GPE using DPV as shown in Fig. 4. DPVs of GPE electrode in a 0.2 M phosphate electrolyte solution of pH 4.0 displayed a broad and
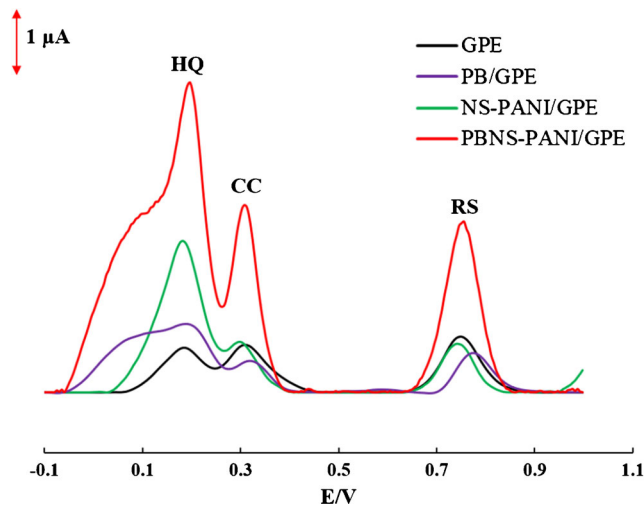
Fig. 4 Differential pulse voltammograms of unmodified and modified GPE in 0.2 M phosphate electrolyte solution (pH 4.0) containing HQ (40 μM), CC (40 μM), and RS (40 μM)

weak oxidation peak for HQ, CC, and RS at 0.20, 0.34 V, and 0.76 V, respectively, whereas for NS-PANI/GPE, the oxidation peaks for HQ, CC, and RS were observed at 0.19, 0.30, and 0.74 V. The peak currents at NS-PANI/GPE increased for HQ, while the peak currents for CC and RS were changed negligibly when compared to GPE. For PB/GPE, broad and weak oxidation peaks for HQ, CC, and RS were visible at 0.21, 0.34, and 0.78 V. In contrast, for the same mixture and conditions, DPV of PBNS-PANI/GPE showed a significant increase in the anodic peak current at 0.20 V, 0.31 V, and 0.76 V for HQ, CC, and RS, respectively, and the peaks became sharper and narrower in comparison to other electrodes.

The results also showed that the PBNS-PANI/GPE improved the sensitivity of three well-separated oxidation peak currents at distinct potentials for the target analytes, which made it suitable for simultaneous detection of three BDIs. The increase in the peak current at PBNS-PANI-PB/GPE was observed to be several times larger than the unmodified GPE, NS-PANI/GPE, and PB/GPE indicating a better transfer of electrons in a mixture of 40 μM of each, BDIs due to good electrical conductivity and enhanced synergistic electrocatalytic activity of PBNS-PANI, which increased the electron transfer kinetics for electrochemical oxidation of HQ, CC, and RS.

Effect of pH and mechanistic insights on the electrooxidation of benzenediol isomers

Since the protons participate in the electrode reaction, the electrooxidation of CC, HQ, and RS can be significantly affected by the acidity of the electrolyte. The effect of pH on the PBNS-PANI/GPE signal showing the electrochemical behavior of the BDI in the pH range of 2.0–8.0 was investigated using DPV as shown in Fig. 5.

The results indicated that as the pH of the solution increased, the anodic peak potentials (E_p) for HQ, CC, and RS displayed a negative shift, emphasizing the involvement of protons during the electrode reaction. The anodic peak potential shift with increasing pH for HQ, CC, and RS followed a linear trend as shown in the following equations:

$$E_p(HQ) = -0.0529\,pH + 0.42\;(R^2 = 0.9931) \tag{2}$$

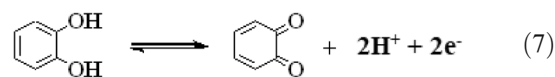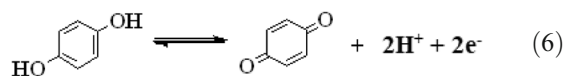$$E_p(CC) = -0.0536\,pH + 0.5336\;(R^2 = 0.9924) \tag{3}$$

$$E_p(RS) = -0.0643\,pH + 1.0114\;(R^2 = 0.9958) \tag{4}$$

The anodic peak potentials for the benzenediol isomers at specific pH were calculated using the following equation [57]:

$$dE_p/dpH = -\frac{2.303mRT}{nF}pH \tag{5}$$

where m and n are the number of protons and electrons involved in the reaction, respectively, and the corresponding Nernstian slope $\left(-\frac{2.303mRT}{nF}\right)$ value is known to be $0.059\left(\frac{m}{n}\right)$ V/pH. Based on Eqs. 2–4, the experimental slopes obtained from the plots of peak potential values versus the pH for HQ, CC, and RS were 0.053, 0.054, and 0.065 V/pH, respectively, which were close to the theoretical Nernstian slope value. These results emphasized that the electrochemical reaction for HQ, CC, and RS should involve equal number of protons and electrons in the electrode reactions. Therefore, using the information obtained from the effect of pH, mechanistic insights into the redox reactions occurring on the surface of PBNS-PANI/GPE for HQ, CC, and RS were suggested in Eqs. 6–8. The illustrations presented in Eqs. 6 and 7 were concluded based on the known two-electron and two-proton exchange occurring during the electrochemical redox reactions between HQ and CC [19, 31].

$$\text{(structure: HO–C}_6\text{H}_4\text{–OH)} \rightleftharpoons \text{(structure: O=C}_6\text{H}_4\text{=O)} + 2H^+ + 2e^- \tag{6}$$

$$\text{(structure: catechol)} \rightleftharpoons \text{(structure: ortho-quinone)} + 2H^+ + 2e^- \tag{7}$$

However, for RS, the resonance between the hydroxyl group and the π electrons was compromised due to its meta-structure, which would impede its oxidation and usually require over-potential to undergo oxidation. RS also undergoes keto-enol tautomerism reaction mechanism that involves the

Fig. 5 **a** Differential pulse voltammograms of PBNS-PANI/GPE showing the effect of pH on the peak separation and peak current for the oxidation of hydroquinone (HQ), catechol (CC), and resorcinol (RS) in 0.2 M phosphate electrolyte solution at various pH (2–8). **b** Plot of anodic peak current versus pH for the three analytes. [HQ], [CC], and [RS] = 40 μM
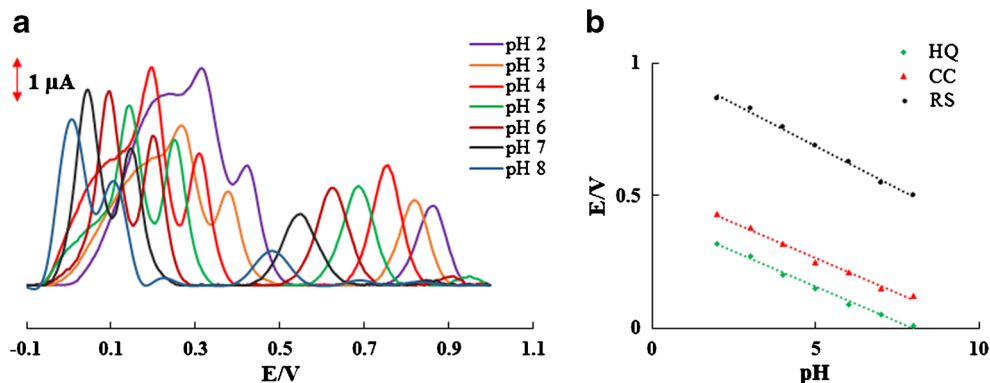
hydroxyl groups of the RS. The reaction mechanism illustrated in Eq. 8 indicates that initially, one electron and one proton are exchanged in the electrochemical redox reaction and this results in formation of three RS radicals which would further react with another RS to form three types (ether, carbon, or peroxide) of dimers [19]. Past research has shown that these three dimers were oxidized more easily compared to the RS monomers [31, 58]. The carbon or ether linked dimers are known to be more predominant as the peroxide linked dimers are not stable and break shortly once they formed [59]. Based on the previous studies, for the phenol containing polymer compounds, carbon linkage was predominantly observed, while for the highly substituted phenol containing polymers, it is the ether linkage which was predominant [19, 60]. It should be noted that additional experiments with sodium acetate buffer, pH 4, were also performed to check the detection

of capability of the PBNS-PANI/GPE modified electrode in simultaneously detecting the BDIs. It was observed that the peak potentials for the BDIs shifted to higher potentials and the oxidation peak current for CC was significantly lower for the sodium acetate buffer at pH 4.0, when compared to the peak potentials and the oxidation peak current obtained while using 0.2 M H_3PO_4 solution at pH 4.0 (Fig. S4, see ESM). This indicated that the buffer ions from acetate buffer would hinder the electrochemical redox conversion. Therefore, all the experimental work in this study was performed using 0.2 M H_3PO_4 electrolyte solution at pH 4.0.

In addition, 0.2 M phosphate electrolyte solution at pH 4.0 was chosen as optimum pH due to the stability of the PBNS-PANI in acidic conditions [39, 40] and for attaining good sensitivity along with maximum linear range during DPV measurements, when compared to Fig. 6.

$$(8)$$
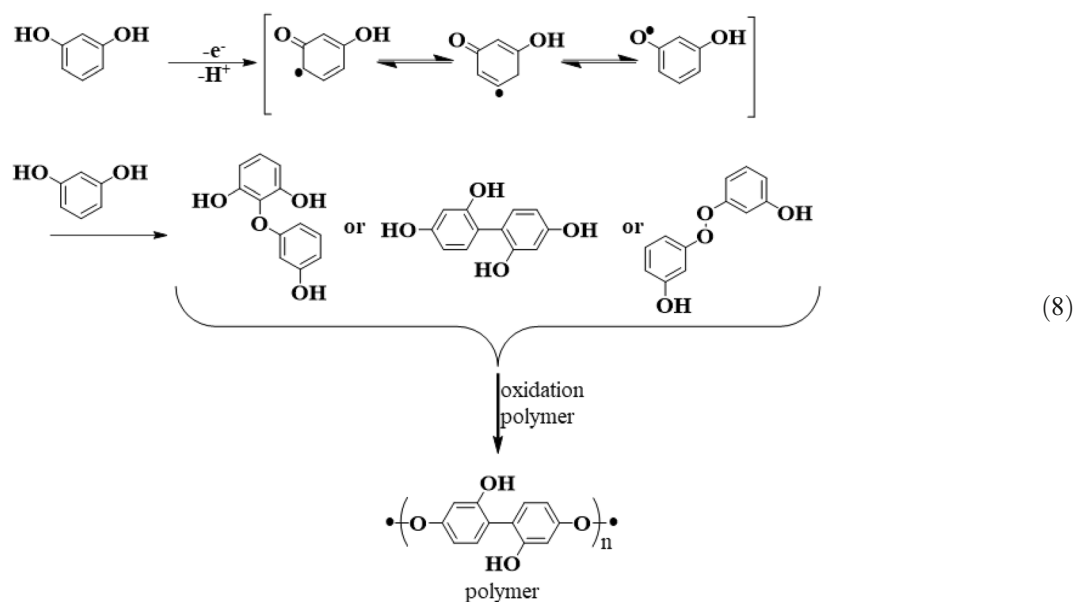
## Standard heterogeneous rate constant (k$_s$) for the electrochemical reactions

Past studies have determined the standard rate constants, k_s, values for different analytes using the Nicholson and Shain theory [61–63]. The effect of different scan rates from 100 to 1500 mV on the anodic and cathodic peak current and potential for the HQ and CC, and from 10 to 1500 mV on anodic peak current and potential for RS was investigated using the PBNS-PANI/GPE. For both HQ and CC, the oxidation peak potential shifted positively, and the reduction peak potential shifted negatively with increasing scan rate. The results for

HQ, CC, and RS were shown in Fig. S5 (see ESM). These results indicated that the oxidation process for HQ and CC was a quasi-reversible electrode process but for RS only, the oxidation peak was observed, which also shifted positively with increasing scan rate. This indicated that for RS, the oxidation process was irreversible at the electrode surface.

For a diffusion-controlled electrochemical process, the standard heterogeneous rate constant (k_s) and charge transfer coefficient (α) for analytes can be calculated by Nicholson-Shain's equation [61]:

$$I_p = 0.227nFAC_ok_sexp\left[(-\alpha nF/RT)\left(E_p-E^o\right)\right] \quad (9)$$

Fig. 6 Differential pulse voltammograms of PBNS-PANI/GPE in 0.2 M phosphate electrolyte solution (pH 4.0) for the simultaneous detection of HQ, CC, and RS at varying concentrations. Insets (B–D) display the plots for the concentration dependence of increasing anodic peak current signals for HQ, CC, and RS with the linear range marked in blue and orange
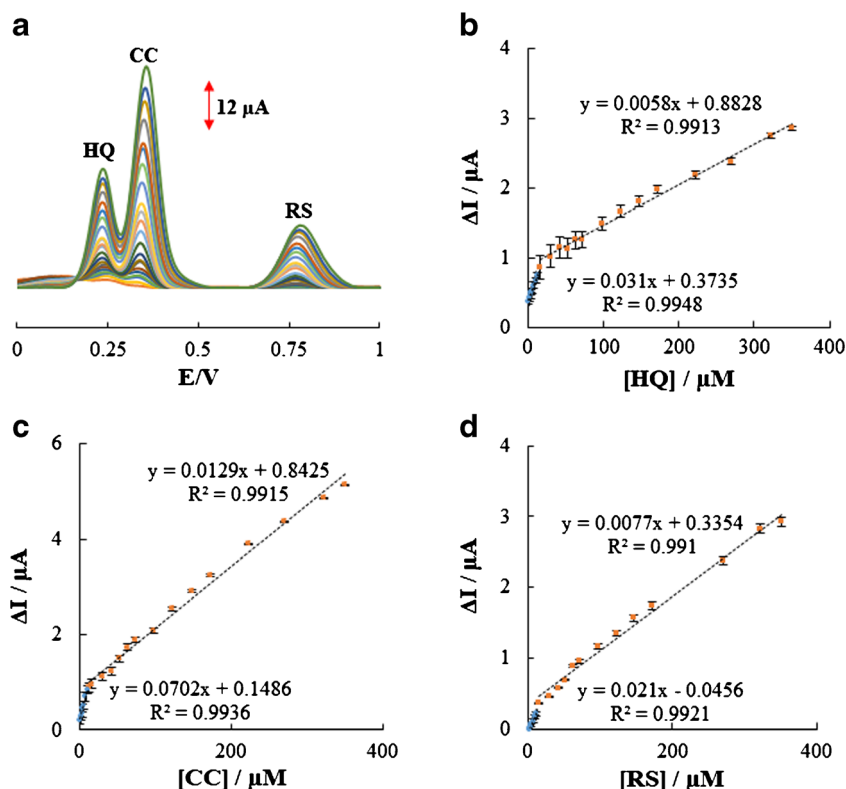
where R is the gas constant, T is the temperature, F is the Faraday's constant, n is the number of electrons taking part in the reaction, C_o is the concentration of the analyte, E_p is the peak potential, and $E°$ is the formal potential.

Based on this equation, the relationship between the peak current and the difference between the peak potential (E_p) and formal potential ($E°$) at different scan rates from the graph of $lnI_p = f(E_p − E^o)$ will give a linear regression (Fig. S5, see ESM). The slope of the straight line will equal to $αnF/RT$, and the intercept of the plot will equal to $0.227nFAC_ok_s$; therefore, the value of charge transfer coefficient, $α$, and the standard heterogeneous rate constants, k_s, can be determined from the slopes and the intercept of the straight line [61–63]. It was determined in the earlier experiments that the number of electrons taking part in the reaction of HQ and CC are 2; therefore, $α$ was determined to be 0.48, 0.45, and 0.66 for HQ, CC, and RS respectively. Moreover, the k_s values are determined to be $9.49 × 10^{−2}$, $3.47 × 10^{−1}$, and $4.76 × 10^{−7}$ cm s$^{−1}$ for HQ, CC, and RS, respectively. The k_s value obtained for HQ using PBNS-PANI/GPE is higher than that observed at CPE ($4.35 × 10^{−4}$ cm s$^{−1}$) [64], ionic liquid (IL)/CPE ($2.38 × 10^{−3}$ cm s$^{−1}$) [64], chemically reduced graphene oxide (CRGO)/GCE ($2.12 × 10^{−2}$ cm s$^{−1}$) [65], thermally reduced graphene oxide (TRGO)/GCE ($1.46 × 10^{−2}$ cm s$^{−1}$) [65], and graphene-chitosan/GCE ($1.47 × 10^{−2}$ cm s$^{−1}$) [66]. Moreover, the k_s value obtained for CC using PBNS-PANI/GPE is higher than that observed at nitrogen-doped hollow carbon spheres (NC)/SPE ($2.31 × 10^{−2}$ cm s$^{−1}$) [67], silver nanoparticles-polydopamine-graphene nanocomposite (AgNPs-Pdop@Gr)/GCE ($2.5 × 10^{−2}$ cm s$^{−1}$) [68], and graphene-chitosan/GCE ($2.1 × 10^{−2}$ cm s$^{−1}$) [66]. These results emphasize that the electron transfer is effectively promoted with the PB-PANI nanocomposite.

Chronoamperometric studies

The working electrode potentials were set at 0.23, 0.34, and 0.74 V vs Ag/AgCl for different concentrations of HQ, CC, and RS respectively, at PBNS-PANI/GPE in

Table 1 Comparison of the calculated diffusion coefficients for hydroquinone (HQ), catechol (CC), and resorcinol (RS) obtained using a modified graphite paste electrode with Prussian blue-polyaniline nanocomposite (PBNS-PANI/GPE) with the ones reported in the literature

(D/cm² s$^{−1}$)			Reference
HQ	CC	RS	
$3.47 × 10^{−5}$	$7.19 × 10^{−5}$	$8.61 × 10^{−5}$	[31]
–	$1.17 × 10^{−6}$	–	[69]
$5.05 × 10^{−4}$	–	–	[70]
$1.85 × 10^{−5}$	$1.84 × 10^{−5}$	–	[71]
$2.77 × 10^{−5}$	–	–	[72]
$1.121 × 10^{−5}$	$9.170 × 10^{−6}$	–	[73]
$2.44 × 10^{−5}$	$1.44 × 10^{−5}$	$4.14 × 10^{−5}$	This work

0.2 M phosphate electrolyte solution (pH 4.0) and the chronoamperometric studies were performed to determine the diffusion coefficients of the BDI. The typical chronoamperograms and the Cottrell plots for the BDI are shown in Figs. S6-S8 (see ESM). The diffusion coefficients for the electroactive analytes were calculated using the Cottrell equation [55]:

$$I = nFAD^{1/2}C_b\pi^{-1/2}t^{-1/2} \tag{10}$$

where n is the number of electrons transferred, F is Faraday's constant (96,485 C mol^{-1}), A is the effective surface area of the electrode, D is the apparent analyte diffusion coefficient, C_b is the bulk concentration (mol cm^{-3}), and t is the time. The Cottrell plot illustrated by the graph of I versus $t^{-1/2}$ showed the variation of current with time that linear due to the diffusion control for the electrochemical reaction under mass transport limited conditions. Furthermore, the slope of the linear region ($nFAD^{1/2}C_b\pi^{-1/2}$) was used to calculate the value of D for the BDI, which were found to be 2.44×10^{-5}, 1.44×10^{-5}, and 4.14×10^{-5} cm^2 s^{-1} for HQ, CC, and RS, respectively. A few studies in the literature have reported D values of HQ, CC, and RS. A comparison of the literature reported values is displayed in Table 1. According to Table 1, the calculated D values from this report are within

acceptable range of the ones reported in the literature.

Calibration curves, detection limits, and simultaneous determination of benzenediol isomers

Under the optimum conditions, the relationship between the oxidation peak currents and the concentration of three benzenediol isomers was studied using the DPV because of its better sensitivity. The voltammograms from the DPV analyses showed the appearance of three well-distinguished oxidation peaks for HQ, CC, and RS (Fig. 6). The plot for the electrocatalytic oxidation peak current of HQ, CC, and RS at the surface of PBNS-PANI/GPE was linearly dependent on the increasing analyte concentrations in two linear segments with two different slopes associated with two different ranges of analyte concentration (Table 2).

Two linear ranges for detection of the BDIs are widely reported [19, 31, 74–76]. Past studies [19, 31] having diffusion-controlled process at their electrode surface has shown two slopes in their calibration curves while simultaneous detection of BDIs. We hypothesized that at low and high concentrations of the analytes, the surface activity of the PBNS-PANI/GPE modified electrode was different, which was responsible for the observed difference in the slopes of two linear segments. A high number of active sites were available on the electrode surface at lower concentrations of the

Table 2 Performance comparison of the modified electrode for HQ, CC, and RS detection with other reported electrochemical systems in literature

Electrode	Linear range/μM			LOD/μM			Ref.
	HQ	CC	RS	HQ	CC	RS	
Graphene-chitosan/GCE	1–300	1–400	1–550	0.75	0.75	0.75	[66]
GC/CNT–RR–NF	1.3–433.3	1.3–433.3	–	0.21	0.18	–	[78]
NRCu-rGO	0.13–131.5	0.13–131.5	0.13–131.5	0.049	0.052	0.060	[31]
Co_3O_4@carbon	0.8–127.1	0.6–116.4	–	0.03	0.03	–	[89]
1D PEDOT-Gr/Ta	1–250	4–300	2–300	0.06	0.08	0.16	[30]
RGO–MWNTs	8–391	5.5–540	–	2.6	1.8	–	[29]
MWCNT@rGONR	15–921	15–1101	15–1301	3.89	1.73	5.77	[77]
Au-Pd NF/rGO/GCE	1.6–100	2.5–100	2.0–100	0.5	0.80	0.70	[79]
GCE/Pd/CuNWs-CNTs	1–99, 99–228	1–280	1–33, 33–228	0.40	0.60	0.80	[80]
GPE/PQ-BNWs	0.76–324.7	0.74–322	4.99–970.7	0.12	0.20	0.82	[19]
NMC-G/GCE	0.5–400	1–300	3–200	0.15	0.3	1.0	[81]
Cu-MOF-GN	1–100	1–100	–	0.59	0.33	–	[82]
Ag/MWCNT/GCE	2.5–260	20–260	–	0.16	0.2	–	[83]
PGCE	10–300	10–300	–	3.57	3.99	–	[84]
Pd/CuNWs-CNTs	1–99, 99–228	1–280	1–33, 33–228	0.40	0.60	0.80	[80]
ZnO-carbon cloth	2–30	2–45	2–385	0.57	0.81	7.20	[85]
AuNPs/CNTs/graphene hybrids	0–80	0–80	0–80	0.80	0.95	0.10	[86]
P-rGO	5–90	5–120	5–90	0.08	0.18	2.62	[87]
AuNPs/Fe_3O_4-APTES-GO/GCE	3–137	2–145	–	1.1	0.8	–	[88]
PBNS-PANI/GPE	1–12.5, 12.5–350.5	1–10, 10–350.5	2–12.5, 12.5–350.5	0.179	0.010	0.02	This work

analytes. However, the number of active sites decreased at higher concentrations of the analytes. The detection limit was derived using the equation $Y_{LOD} = 3S_{bk}/m$, where Y_{LOD} is the signal for limit of detection, S_{bk} is the standard deviation of the blank signal, and m is the slope of the calibration curve for the corresponding analyte. The theoretical limit of detection (LOD) for HQ, CC, and RS was calculated to be 0.18, 0.01, and 0.02 μM, respectively. The electrocatalytic properties, unique redox properties, and the high electron transfer kinetics due to the increased surface area of the electroactive polymer obtained from the PBNS-PANI nanocomposite allowed for the significant electrochemical performance of the modified electrode to achieve good detection limits.

Furthermore, stability of the PBNS-PANI/GPE modified electrodes was investigated by using them to measure DPV signals for simultaneous detection of HQ, CC, and RS for a period of 1 month in 0.2 M phosphate electrolyte solution (pH 4.0). DPV signals were recorded using the same concentration of the benzenediol isomers. The excellent stability of the PBNS-PANI/GPEs was emphasized by the retained peak potential and the peak current (ΔI_{pa}) values for HQ, CC, and RS at 94.29%, 95.63%, and 97.88%, respectively. In addition, the repeatability of the PBNS-PANI/GPE was studied using the DPV technique for 9 successive trials by simultaneously detecting HQ, CC, and RS. The results shown in Fig. S9 (see ESM) emphasize that the relative standard deviations of the results were 3.26, 1.64, and 3.27% for HQ, CC, and RS, respectively. These results confirm the excellent stability and repeatability for the PBNS-PANI/GPE in simultaneous determination of HQ, CC, and RS.

The performance of PBNS-PANI/GPE electrode for simultaneous determination of HQ, CC, and RS was also compared to the recently published work in literature showing simultaneous determination of benzenediol isomers (Table 2). As shown in Table 2, the merits of our proposed sensor in terms of LOD are comparable or better than some of the recently reported sensors in the literature, especially for RS. Moreover,

the mechano-synthesis method used in preparation of PBNS-PANI/GPE is advantageous as it was a robust, easily reproducible, simple, and cost-effective process. The linear range for PBNS-PANI/GPE when compared to the work reported by Yang et al. [77] and by Hu et al. [29] is low, but it can detect at much lower concentrations than both the studies. In addition, PBNS-PANI/GPE exhibited better LOD to the one reported by both Yang et al. [77] and Hu et al. [29]. However, as shown in Table 2, PBNS-PANI/GPE was also significantly better in both LOD and linear range than the other modifiers reported recently in literature. This, along with the other discrepancies in performance comparison of different electrode modifiers in Table 2, further shows that it is still essential to investigate and find novel electrode materials for simultaneous determination of trace level of BDIs.

Interference studies

As BDI, HQ, CC, and RS generally co-exist in environmental samples, it was imperative to perform the interference studies for the selective determination of one of the isomers from an interfering matrix of other electroactive compounds that were oxidized under the same or near identical conditions. In each of experiment, the concentration of one of the isomers was varied, while the concentrations of the other two isomers were held constant (Fig. S10, see ESM). For example, in ESM Fig. S10(A), the oxidation peak current for HQ was increased with increasing concentrations of HQ, while the concentration of CC and RS was held constant. Moreover, the peak current for CC and RS did not show any enhancement as observed with HQ. Similarly, when the respective experiments were performed with CC (ESM Fig. S10(B), and RS (ESM Fig. S10(C), the peak currents for the respective species increased with increasing concentrations, while the peak current for the other two species were constant at their respective constant concentrations. Therefore, we conclude that the oxidation of

Table 3 Simultaneous determination of HQ, CC, and RS in creek water, commercial hair dye, and commercial whitening cream samples ($n = 3$). "Detected" is the quantity of analyte(s) already existing in the sample, "spiked" is the total standard solution of the analyte that was added to the sample, and "found" is the quantity of spiked analyte concentration that was calculated from the solution which was spiked

Sample	Analyte	Detected (μM)	Spiked (μM)	Found (μM)	Recovery (%)
Creek water	HQ	–	160	155.80 ± 0.05	97.42 ± 0.05
	CC	–	60	58.57 ± 0.04	97.62 ± 0.04
	RS	–	160	154.22 ± 0.03	96.39 ± 0.03
1% (w/v) commercial hair dye	HQ	–	15	14.78 ± 0.13	98.51 ± 0.13
	CC	–	5	4.50 ± 0.05	90.01 ± 0.05
	RS	12.02 ± 0.32	5	5.02 ± 0.03	100.50 ± 0.03
1% (w/v) commercial whitening cream	HQ	–	35	32.92 ± 0.08	94.07 ± 0.08
	CC	–	20	21.19 ± 0.02	105.97 ± 0.02
	RS	–	20	19.32 ± 0.13	96.58 ± 0.13

HQ, CC, and RS at PBNS-PANI/GPE was independent of each other and did not cause significant interference.

Real samples

The practicality and the potential of the proposed electrochemical sensor based on PBNS-PANI/GPE modified electrode was investigated for simultaneous determination of HQ, CC, and RS in commercial hair dyes, skin whitening cream, and creek water. As indicated in Table 3, DPV responses from the respective samples of known concentrations diluted in 0.2 M phosphate electrolyte solution were used for simultaneous determination of HQ, CC, and RS using the spike and recovery method. As shown in Table 3, the acceptable recovery values obtained from different matrices implied the potential applicability of the described sensor in the determination of BDI for on-filed applications using real samples.

Conclusions

Herein, we developed a novel PBNS-PANI/GPE using mechano-synthesis method directly from aniline and iron(III) chloride salt for the first time, to the best of our knowledge. As a proof-of-concept study, the PBNS-PANI/GPE was used for speciation of HQ, CC, and RS. The PBNS-PANI nanocomposite was instrumental in obtaining a wide linear range with high selectivity of HQ, CC, and RS. The results indicated that PBNS-PANI/GPE not only had the most effective surface area, which allowed for enhanced peak current signals and the kinetics for oxidation of the BDI, but also produced well-defined peak separations during the speciation of HQ, CC, and RS. Finally, PBNS-PANI/GPE was successfully applied for simultaneous determination of the HQ, CC, and RS in real samples with excellent recovery results. Overall, we conclude that PBNS-PANI/GPE can provide a promising platform for electrochemical sensor applications.

Compliance with ethical standards

References

1. Wang HF, Wu YY, Yan XP. Room-temperature phosphorescent discrimination of catechol from resorcinol and hydroquinone based on sodium tripolyphosphate capped Mn-doped ZnS quantum dots. Anal Chem. 2013;85:1920–5.

2. Yu Z, Wang H, Bai B, Qu S, Li F, Ran X, et al. A novel pyromellitic diimide derivative: synthesis, gelation and spontaneous colorimetric sensing of dihydroxybenzene isomers. Mater Sci Eng C. 2010;30:699–704.

3. Shi B, Su Y, Zhao J, Liu R, Zhao Y, Zhao S. Visual discrimination of dihydroxybenzene isomers based on a nitrogen-doped graphene quantum dot-silver nanoparticle hybrid. Nanoscale. 2015;7:17350–8.

4. Suresh S, Srivastava VC, Mishra IM. Adsorption of catechol, resorcinol, hydroquinone, and their derivatives: a review. Int J Energy Environ Eng. 2012;3:32.

5. Fahimi-Kashani N, Hormozi-Nezhad MR. Gold nanorod-based chrono-colorimetric sensor arrays: a promising platform for chemical discrimination applications. ACS Omega. 2018;3:1386–94.

6. Yang H, Zha J, Zhang P, Qin Y, Chen T, Ye F. Fabrication of CeVO4as nanozyme for facile colorimetric discrimination of hydroquinone from resorcinol and catechol. Sensors Actuators B. 2017;247:469–78.

7. Cao X, Cai X, Feng Q, Jia S, Wang N. Ultrathin CdSe nanosheets: synthesis and application in simultaneous determination of catechol and hydroquinone. Anal Chim Acta. 2012;752:101–5.

8. Milligan PW, Hãggblom MM. Biodegradation of resorcinol and catechol by denitrifying enrichment cultures. Environ Toxicol Chem. 1998;14:1456–61.

9. Health Canada (2018) Catechol. https://www.canada.ca/en/health-canada/services/chemical-substances/challenge/batch-1/catechol.html. Accessed 15 Oct 2018.

10. Health Canada (2018) Hydroquinone. https://www.canada.ca/en/health-canada/services/chemical-substances/challenge/batch-1/hydroquinone.html. Accessed 15 Oct 2018.

11. Health Canada (2018) Cosmetic ingredient hotlist. https://www.canada.ca/en/health-canada/services/consumer-product-safety/cosmetics/cosmetic-ingredient-hotlist-prohibited-restricted-ingredients/hotlist.html. Accessed 15 Oct 2018.

12. van Duursen MBM, Sanderson JT, de Jong PC, Kraaij M, van den Berg M. Phytochemicals inhibit catechol-O-methyltransferase activity in cytosolic fractions from healthy human mammary tissues: implications for catechol estrogen-induced DNA damage. Toxicol Sci. 2004;8:316–24.

13. Feng X, Gao W, Zhou S, Shi H, Huang H, Song W. Discrimination and simultaneous determination of hydroquinone and catechol by tunable polymerization of imidazolium-based ionic liquid on multi-walled carbon nanotube surfaces. Anal Chim Acta. 2013;805:36–44.

14. Capasso R, Evidente A, Schivo L, Orru G, Marcialis MA, Cristinzio G. Antibacterial polyphenols from olive oil mill waste waters. J Appl Microbiol. 1995;79:393–8.

15. Boyd GE, Schubert J, Adamson AW. The exchange adsorption of ions from aqueous solutions by organic zeolites. Ion-exchange Equilibria. J Am Chem Soc. 1947;69:2836–48.

16. Zargar B, Hatamie A. Colorimetric determination of resorcinol based on localized surface plasmon resonance of silver nanoparticles. Analyst. 2012;137:5334–8.

17. Saha S, Mistri R, Ray BC. A rapid and selective method for simultaneous determination of six toxic phenolic compounds in mainstream cigarette smoke using single-drop microextraction followed by liquid chromatography-tandem mass spectrometry. Anal Bioanal Chem. 2013;405:9265–72.

18. Minero C, Vincenti M, Lago S, Pelizzetti E. Determination of trace amounts of highly hydrophilic compounds in water by direct derivatization and gas chromatography - mass spectrometry. Fresenius J Anal Chem. 1994;350:403–9.

19. Tohidinia M, Farsadrooh M, Bahmanzadeh S, Sabbaghi N, Noroozifar M. Poly(quercetin)-bismuth nanowires as a new modifier for simultaneous voltammetric determination of dihydroxybenzene isomers and nitrite. RSC Adv. 2018;8:1237–45.

20. Garoz-Ruiz J, Izquierdo D, Colina A, Palmero S, Heras A. Optical fiber spectroelectrochemical device for detection of catechol at press-transferred single-walled carbon nanotubes electrodes. Anal Bioanal Chem. 2013;405:3593–602.

21. Haghighi B, Dadashvand R. Flow injection chemiluminescence analysis of phenolic compounds using the NCS-luminol system. Anal Bioanal Chem. 2006;384:1246–53.

22. Pistonesi M, Centurión ME, Pereyra M, Lista AG, Band BSF. Synchronous fluorescence for simultaneous determination of hydroquinone and resorcinol in air samples. Anal Bioanal Chem. 2004;378:1648–51.

23. Dong S, Chi L, Zhang S, He P, Wang Q, Fang Y. Simultaneous determination of phenylenediamine isomers and dihydroxybenzene isomers in hair dyes by capillary zone electrophoresis coupled with amperometric detection. Anal Bioanal Chem. 2008;391:653–9.

24. Wei H, Hossein Abtahi SM, Vikesland PJ. Plasmonic colorimetric and SERS sensors for environmental analysis. Environ Sci Nano. 2015;2:120–35.

25. Lisdat F, Wollenberger U, Makower A, Hörtnagl H, Pfeiffer D, Scheller FW. Catecholamine detection using enzymatic amplification. Biosens Bioelectron. 1997;12:1199–211.

26. Mizutani F, Yabuki S, Asai M. Highly-sensitive measurement of hydroquinone with an enzyme electrode. Biosens Bioelectron. 1991;6:305–10.

27. Morita M, Iwasaki Y, Horiuchi T, Niwa O. Selective electrochemical detection of catechol and catecholamines on modified electrodes with molecular template. Denki Kagaku. 1996;64:1239–43.

28. Morita M, Niwa O, Horiuchi T. Interdigitated array microelectrodes as electrochemical sensors. Electrochim Acta. 1997;42:3177–83.

29. Hu F, Chen S, Wang C, Yuan R, Yuan D, Wang C. Study on the application of reduced graphene oxide and multiwall carbon nanotubes hybrid materials for simultaneous determination of catechol, hydroquinone, p-cresol and nitrite. Anal Chim Acta. 2012;724:40–6.

30. Tian F, Li H, Li M, Li C, Lei Y, Yang B. Synthesis of one-dimensional poly(3,4-ethylenedioxythiophene)-graphene composites for the simultaneous detection of hydroquinone, catechol, resorcinol, and nitrite. Synth Met. 2017;226:148–56.

31. Sabbaghi N, Noroozifar M. Nanoraspberry-like copper/ reduced graphene oxide as new modifier for simultaneous determination of benzenediols isomers and nitrite. Anal Chim Acta. 2019;1056: 16–25.

32. Yin T, Wei W, Zeng J. Selective detection of dopamine in the presence of ascorbic acid by use of glassy-carbon electrodes modified with both polyaniline film and multi-walled carbon nanotubes with incorporated β-cyclodextrin. Anal Bioanal Chem. 2006;386:2087–94.

33. Gautam V, Singh KP, Yadav VL. Polyaniline/MWCNTs/starch modified carbon paste electrode for non-enzymatic detection of

34. cholesterol: application to real sample (cow milk). Anal Bioanal Chem. 2018;410:2173–81.

34. Bartlett PN, Ling-Chung SK. Conducting polymer gas sensors part III: results for four different polymers and five different vapours. Sensors Actuators. 1989;20:287–92.

35. Kilmartin PA, Martinez A, Bartlett PN. Polyaniline-based microelectrodes for sensing ascorbic acid in beverages. Curr Appl Phys. 2008;8:320–3.

36. Suprun E, Evtugyn G, Budnikov H, Ricci F, Moscone D, Palleschi G. Acetylcholinesterase sensor based on screen-printed carbon electrode modified with prussian blue. Anal Bioanal Chem. 2005;383:597–604.

37. Karyakin AA, Gitelmacher OV, Karyakina EE. A high-sensitive glucose amperometric biosensor based on prussian blue modified electrodes. Anal Lett. 1994;27:2861–9.

38. Buleandra M, Rabinca AA, Mihailciuc C, Balan A, Nichita C, Stamatin I, et al. Screen-printed Prussian blue modified electrode for simultaneous detection of hydroquinone and catechol. Sensors Actuators B. 2014;203:824–32.

39. Amarnath CA, Sawant SN. Tailoring synthesis strategies for polyaniline-prussian blue composite in view of energy storage and H2O2 sensing application. Electrochim Acta. 2019;295:294–301.

40. Thakur B, Sawant SN. Polyaniline/prussian-blue-based amperometric biosensor for detection of uric acid. Chempluschem. 2013;78:166–74.

41. Molapo KM, Ndangili PM, Ajayi RF, Mbambisa G, Mailu SM, Njomo N, et al. Electronics of conjugated polymers (I): polyaniline. Int J Electrochem Sci. 2012;7:11859–75.

42. Huang WS, MacDiarmid AG. Optical properties of polyaniline. Polymer (Guildf). 1993;34:1833–45.

43. Shimano JY, MacDiarmid AG. Polyaniline, a dynamic block copolymer: key to attaining its intrinsic conductivity? Synth Met. 2001;123:251–62.

44. Nicolas-Debarnot D, Poncin-Epaillard F. Polyaniline as a new sensitive layer for gas sensors. Anal Chim Acta. 2003;475:1–15.

45. De Albuquerque JE, Mattoso LHC, Faria RM, Masters JG, MacDiarmid AG. Study of the interconversion of polyaniline oxidation states by optical absorption spectroscopy. Synth Met. 2004;146:1–10.

46. Farrokhzadeh A, Modarresi-Alam AR. Complete doping in solid-state by silica-supported perchloric acid as dopant solid acid: synthesis and characterization of the novel chiral composite of poly [(±)-2-(sec-butyl) aniline]. J Solid State Chem. 2016;237:258–68.

47. Bhadra S, Khastgir D, Singha NK, Lee JH. Progress in preparation, processing and applications of polyaniline. Prog Polym Sci. 2009;34:783–810.

48. Yu J, Chen Y, Wuhrer R, Liu Z, Ringer SP. In situ formation of BN nanotubes during nitriding reactions. Chem Mater. 2005;17:5172–6.

49. Sawant SN, Bagkar N, Subramanian H, Yakhmi JV. Polyaniline-prussian blue hybrid: synthesis and magnetic behaviour. Philos Mag. 2004;84:2127–38.

50. Tang Z, Liu S, Wang Z, Dong S, Wang E. Electrochemical synthesis of polyaniline nanoparticles. Electrochem Commun. 2000;2:32–5.

51. Wei XL, Fahlman M, Epstein AJ. XPS study of highly sulfonated polyaniline. Macromolecules. 1999;32:3114–7.

52. Muthusamy S, Charles J. In situ synthesis and characterization of polyaniline/prussian blue/zinc oxide nanocomposite. Polym Bull. 2019;76:119–37.

53. Zou Y, Wang Q, Xiang C, She Z, Chu H, Qiu S, et al. One-pot synthesis of ternary polypyrrole-Prussian-blue-graphene-oxide hybrid composite as electrode material for high-performance supercapacitors. Electrochim Acta. 2016;188:126–34.

54. Zhang J, Gao J, Song Q, Guo Z, Chen A, Chen G, et al. N-substituted carboxyl polyaniline covalent grafting reduced

graphene oxide nanocomposites and its application in supercapacitor. Electrochim Acta. 2016;199:70–9.

55. Ganesh HVS, Noroozifar M, Kerman K. Epigallocatechin gallate-modified graphite paste electrode for simultaneous detection of redox-active biomolecules. Sensors. 2018;18:23.

56. Lee SH, Fang HY, Chen WC, Lin HM, Chang CA. Electrochemical study on screen-printed carbon electrodes with modification by iron nanoparticles in Fe(CN)64−/3- redox system. Anal Bioanal Chem. 2005;383:532–8.

57. Liu CY, Yao JP, Tang HW, Zhu SP, Hu JF. The electrochemical behavior of p-benzenediol on a self-assembled monolayers Pt electrode modified with N-(2-mercapto-1,3,4-thiadiazol-5-yl)- N′-(4-substituted-arylacetyl) urea. Anal Bioanal Chem. 2006;386:1905–11.

58. Yi H, Wu K, Hu S, Cui D. Adsorption stripping voltammetry of phenol at Nafion-modified glassy carbon electrode in the presence of surfactants. Talanta. 2001;55:2001.

59. Bach RD, Ayala PY, Schlegel HB. A reassessment of the bond dissociation energies of peroxides. An ab initio study. J Am Chem Soc. 1996;118:12758–65.

60. Gattrell M. A Fourier transform infrared spectroscopy study of the passive film produced during aqueous acidic phenol electro-oxidation. J Electrochem Soc. 1992;139:2736–44.

61. Nicholson RS, Shain I. Theory of stationary electrode polarography: single scan and cyclic methods applied to reversible, irreversible, and kinetic systems. Anal Chem. 1964;36:706–23.

62. Corona-Avendaño S, Alarcón-Angeles G, Ramírez-Silva MT, Rosquete-Pina G, Romero-Romo M, Palomar-Pardavé M. On the electrochemistry of dopamine in aqueous solution. Part I: the role of [SDS] on the voltammetric behavior of dopamine on a carbon paste electrode. J Electroanal Chem. 2007;609:17–26.

63. Khan SI, Tadi KK, Chillawar RR, Motghare RV. Interfacing electrochemically reduced graphene oxide with poly(erichrome black T) for simultaneous determination of epinephrine, uric acid and folic acid. J Electrochem Soc. 2018;165:B804–13.

64. Zhang Y, Zheng J Bin (2007) Comparative investigation on electrochemical behavior of hydroquinone at carbon ionic liquid electrode, ionic liquid modified carbon paste electrode and carbon paste electrode. Electrochim Acta 52:7210–7216.

65. Li SJ, Xing Y, Deng DH, Shi MM, Guan PP. A comparative study of different types of reduced graphene oxides as electrochemical sensing platforms for hydroquinone and catechol. J Solid State Electrochem. 2015;19:861–70.

66. Yin H, Zhang Q, Zhou Y, Ma Q, Liu T, Zhu L, et al. Electrochemical behavior of catechol, resorcinol and hydroquinone at graphene-chitosan composite film modified glassy carbon electrode and their simultaneous determination in water samples. Electrochim Acta. 2011;56:2748–53.

67. Long W, Xie Y, Shi H, Ying J, Yang J, Huang Y, et al. Preparation of nitrogen-doped hollow carbon spheres for sensitive catechol electrochemical sensing. Fullerenes Nanotubes Carbon Nanostruct. 2018;26:856–62.

68. Huang KJ, Wang L, Li J, Yu M, Liu YM. Electrochemical sensing of catechol using a glassy carbon electrode modified with a composite made from silver nanoparticles, polydopamine, and graphene. Microchim Acta. 2013;180:751–7.

69. Krampa FD, Aniweh Y, Awandare GA, Kanyong P. A disposable amperometric sensor based on high-performance PEDOT:PSS/ionic liquid nanocomposite thin film-modified screen-printed electrode for the analysis of catechol in natural water samples. Sensors. 2017;17:1716.

70. She Y, Tang Y, Liu H, He P. Electrochemical determination of hydroquinone using hydrophobic ionic liquid-type carbon paste electrodes. Chem Cent J. 2010;4:17.

71. Peng J, Gao ZN. Influence of micelles on the electrochemical behaviors of catechol and hydroquinone and their simultaneous determination. Anal Bioanal Chem. 2006;384:1525–32.

72. Salazar R, Vidal J, Martínez-Cifuentes M, Araya-Maturana R, Ramírez-Rodríguez O. Electrochemical characterization of hydroquinone derivatives with different substituents in acetonitrile. New J Chem. 2015;39:1237–46.

73. Zhang M, Ge C, Jin Y, Hu L, Mo H, Li X, et al. Sensitive and simultaneous determination of hydroquinone and catechol in water using an anodized glassy carbon electrode with polymerized 2-(phenylazo) chromotropic acid. J Chem. 2019;2019:2327064.

74. Lopa NS, Rahman MM, Jang H, Sutradhar SC, Ahmed F, Ryu T, et al. A glassy carbon electrode modified with poly(2,4-dinitrophenylhydrazine) for simultaneous detection of dihydroxybenzene isomers. Microchim Acta. 2018;185:23.

75. Ma G, Xu H, Wu M, Wang L, Wu J, Xu F. A hybrid composed of MoS2, reduced graphene oxide and gold nanoparticles for voltammetric determination of hydroquinone, catechol, and resorcinol. Microchim Acta. 2019;186:689.

76. Gao J, Fang J, Ju X, Zhu W, Lin X, Zhang S, et al. Hierarchical self-assembly of cyclodextrin and dimethylamino-substituted arylene-ethynylene on N-doped graphene for synergistically enhanced electrochemical sensing of dihydroxybenzene isomers. ACS Appl Mater Interfaces. 2017;44:38802–13.

77. Yang S, Yang M, Liu Q, Wang X, Fa H, Wang Y, et al. An ultrasensitive electrochemical sensor based on multiwalled carbon nanotube@reduced graphene oxide nanoribbon composite for simultaneous determination of hydroquinone, catechol and resorcinol. J Electrochem Soc. 2019;166:B547–53.

78. Foroughi MM, Noroozifar M, Khorasani-Motlagh M. Simultaneous determination of hydroquinone and catechol using a modified glassy carbon electrode by ruthenium red/carbon nanotube. J Iran Chem Soc. 2015;12:1139–47.

79. Chen Y, Liu X, Zhang S, Yang L, Liu M, Zhang Y, et al. Ultrasensitive and simultaneous detection of hydroquinone, catechol and resorcinol based on the electrochemical co-reduction prepared Au-Pd nanoflower/reduced graphene oxide nanocomposite. Electrochim Acta. 2017;231:677–85.

80. Sabbaghi N, Noroozifar M, Tohidinia M, Farsadrooh M. Modified glassy carbon electrode with galvanized copper nanowires by palladium and carbon nanotubes for speciation of dihydroxybenzene isomers. Int J Electrochem Sci. 2017;12:8777–92.

81. Peng C, Li Z, Zhang X, Zhou S, Zhang W, Liu X, et al. Simultaneous determination of hydroquinone, catechol and resorcinol with high selectivity based on hollow nitrogen-doped mesoporous carbon spheres decorated graphene. J Electrochem Soc. 2018;165:B212–9.

82. Li J, Xia J, Zhang F, Wang Z, Liu Q. An electrochemical sensor based on copper-based metal-organic frameworks-graphene composites for determination of dihydroxybenzene isomers in water. Talanta. 2018;181:80–6.

83. Goulart LA, Gonçalves R, Correa AA, Pereira EC, Mascaro LH. Synergic effect of silver nanoparticles and carbon nanotubes on the simultaneous voltammetric determination of hydroquinone, catechol, bisphenol A and phenol. Microchim Acta. 2018;185:12.

84. Zhang H, Li S, Zhang F, Wang M, Lin X, Li H. Simultaneous detection of hydroquinone and catechol on electrochemical-activated glassy carbon electrode by simple anodic and cathodic polarization. J Solid State Electrochem. 2017;21:735–45.

85. Meng S, Hong Y, Dai Z, Huang W, Dong X. Simultaneous detection of dihydroxybenzene isomers with ZnO nanorod/carbon cloth electrodes. ACS Appl Mater Interfaces. 2017;9:12453–60.

86. Chen T-W, Yu X-N, Li S-J. Simultaneous determination of dihydroxybenzene isomers using glass carbon electrode modified with 3D CNT-graphene decorated with au nanoparticles. Int J Electrochem Sci. 2019;14:7037–46.

87. Zhang H, Bo X, Guo L. Electrochemical preparation of porous graphene and its electrochemical application in the simultaneous determination of hydroquinone, catechol, and resorcinol. Sensors Actuators B. 2015;220:919–26.

88. Erogul S, Bas SZ, Ozmen M, Yildiz S. A new electrochemical sensor based on Fe3O4 functionalized graphene oxide-gold nanoparticle composite film for simultaneous determination of catechol and hydroquinone. Electrochim Acta. 2015;186:302–13.

89. Zhou T, Gao W, Gao Y, Wang Q. Simultaneous determination of catechol and hydroquinone using non-enzymatic Co3O4@carbon core/shell composites based sensor. J Electrochem Soc. 2019;166 (12):B1069-78.